Spatial Structure of Volume Recombination in JT-60U Detached Divertor Plasmas*)

Kayoko FUJIMOTO, Tomohide NAKANO, Hirotaka KUBO, Keiji SAWADA[1)], Tomonori TAKIZUKA, Hisato KAWASHIMA, Katsuhiro SHIMIZU and Nobuyuki ASAKURA

Japan Atomic Energy Agency, Ibaraki 311–0193, Japan
[1)]*Shinshu University, Nagano 380–8553, Japan*

(Received 9 March 2009 / Accepted 8 April 2009)

Two-dimensional distributions of D_α, D_β, D_γ and D_δ are reconstructed from line-integral measurements. The two-dimensional emission ratio of D_δ to D_γ indicates that the volume recombination occurs throughout the inner divertor plasma. In particular, at an emission peak above the inner strike point, it is shown that the population density of high n levels (n = 4, 5 and 6) is determined by the electron-ion volume recombination with an electron temperature and density of 0.2-0.5 eV and 1×10^{20} m^{-3}, respectively, and that the population density of the n=3 level is not explained by the recombining plasma component with or without the ionizing plasma component.

Keywords: divertor detachment, volume recombination, tomography, spectroscopic measurement, collisional-radiative model, JT-60U

DOI: 10.1585/pfr.4.025

1. Introduction

Heat and particle control is one of the essential means for mitigating damage to plasma-facing components in fusion devices. A poloidal divertor is one of the most promising methods for achieving this control. In particular, creating detached divertor plasmas is a promising operation scenario of a divertor tokamak reactor, because volume recombination dissipates the plasma flowing onto the divertor plates, leading to significant reduction of heat and particle load [1, 2].

In detached divertor plasmas, hydrogen atoms are produced by the volume recombination at the same time hydrogen ions are produced by the ionization [3–5]. These reactions occur predominantly at different spatial zones. Hence investigating this complicated spatial structure of the detached divertor plasmas is of interest and significance for plasma transport studies and fusion research development.

In studies of detached divertor plasmas, line-integral spectroscopic measurement has been performed [3–6]. The electron temperature evaluated from the intensity ratios of the Balmer-series lines from highly excited levels was ~0.5 eV, the electron density evaluated from the spectral line broadening was $\sim 1 \times 10^{20}$ m^{-3}, and the volume recombination flux was roughly equal to the ionization flux [7]. However, two-dimensional distributions of these physical quantities were not investigated.

In this paper, two-dimensional spectroscopic measurement was performed for the deuterium Balmer-series lines in detached divertor plasmas. By using an improved tomographic reconstruction code [8], two-dimensional spatial distributions of the Balmer-series line emissions were reconstructed from the line-integral intensities in order to investigate the spatial distribution of plasma parameters and ionization/recombination zones.

2. Experimental

2.1 Diagnostics

Figure 1 (a) shows a schematic view of a cross-section of the JT-60U tokamak, and Fig. 1 (b) an enlarged view of a cross-section of the divertor region. The divertor region was covered by 60 vertical (1-60 ch) and 32 horizontal (61-92 ch) viewing chords with a spatial resolution of about 1 cm. The divertor dome interrupted 17 viewing chords of the horizontal array, and only the outer divertor plasma was observed with these viewing chords. The emissions from the divertor plasma were transmitted through optical fibers with a core diameter of 200 μm over a distance of ~300 m to a visible spectrometer with a charge-coupled device (CCD) detector [9]. The focal length, the groove density and the inverse linear dispersion of the spectrometer were 0.2 m, 300 grooves/mm and 16 nm/mm, respectively. The full width at half maximum (FWHM) of the instrumental width at an entrance slit of 30 μm was 0.72 nm, and the covered spectral range 350-800 nm. A band reduction filter with a central wavelength of 656 nm, an FWHM of 30 nm and a transmittance at 656 nm of 6% was installed inside the spectrometer to reduce the D_α intensity in particular. The CCD detector had a 26.8×26.0 mm^2 imaging area with a pixel size of 20×20 μm^2, and the quantum ef-

author's e-mail: nakano.tomohide@jaea.go.jp

*) This article is based on the invited talk at the 24th JSPF Annual Meeting (2007, Himeji).

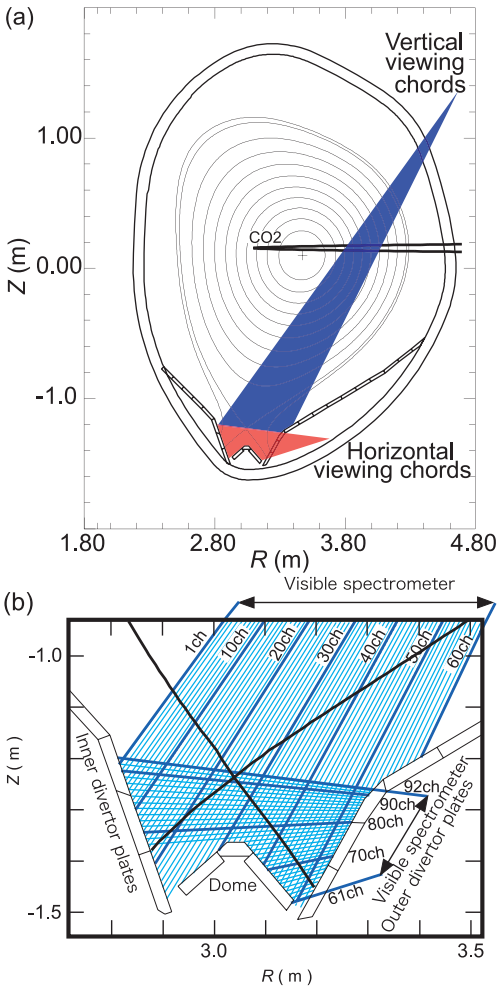

Fig. 1 (a) A schematic view of a poloidal cross-section of JT-60U and (b) an enlarged view of the divertor region. The magnetic configuration at t = 6.0 s of the discharge shown in Fig. 2 and the viewing chords for the CO_2 LASER interferometer and the visible spectrometer are shown.

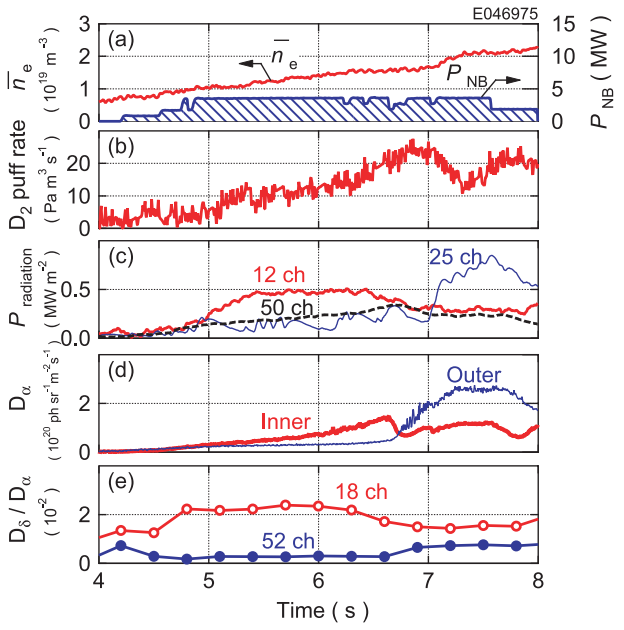

Fig. 2 Waveforms of (a) the line-averaged electron density and the neutral beam injection power, (b) the deuterium gas-puff rate, (c) the radiation power from the inner divertor, the X-point and the outer divertor (12, 25 and 50 ch respectively), (d) the line-integrated intensity of the D_α line emission from the inner and the outer divertor (thick and thin line, respectively) and (e) the ratio of the D_δ line emission to the D_α line emission of 18 ch (line and open circles) and of 52 ch (line and closed circles).

ficiency was ~93% at a wavelength of 550 nm. The frame rate of the CCD detector was set at 300 ms with an exposure time of 25 ms.

Figure 1 (a) also shows the viewing chord of the CO_2 LASER interferometer, which measured the line-averaged electron density. The bolometer viewing chords were similar to the vertical viewing chords of the visible spectrometer, although the spatial resolution was ~4 cm. Hereafter a viewing chord of the bolometer is labeled with the number of the corresponding viewing chord of the vertical array for the visible spectrometer.

2.2 Discharge

The present measurement was performed in an L-mode discharge with a toroidal magnetic field of 3.6 T, a plasma current of 0.8 MA, a safety factor at the 95% poloidal flux surface of 7.0, a major radius of 3.4 m, a minor radius of 0.9 m, a plasma volume of 62 m^3, a triangularity of 0.34 and an ellipticity of 1.3. As shown in Figs. 2 (a) and (b), during a neutral beam injection at 3.5 MW, with increase in the D_2 puff-rate controlled by a feed-back control technique, the core line-averaged electron density increased. With increase in core line-averaged electron density, the radiation profile of the divertor changed as shown in Fig. 2 (c). First, the radiation power along 12 ch was the highest. As shown in Fig. 2 (e), the intensity ratio of D_δ to D_α on 18 ch, which viewed the inner strike point, was already high. This indicates that low temperature and highly radiative plasma was formed at the inner divertor and that the plasma at the inner strike point was detached. Then, the radiation power at the inner divertor started to decrease at t ~ 6.5 s and the radiation peak moved toward the X-point (25 ch), suggesting X-point MARFE. Similarly, in the outer divertor plasma, after 6.7 s, the radiation peak moved toward the X-point and the intensity ratio of D_δ to D_α increased, suggesting detachment of the outer divertor plasma. In the present work, plasma detached at the inner divertor but attached at the outer divertor at t = 6.0 s was analyzed.

3. Analysis

3.1 Tomographic reconstruction

Defects of viewing chords are issues in tomographic reconstruction. In the JT-60U divertor, the dome interrupts

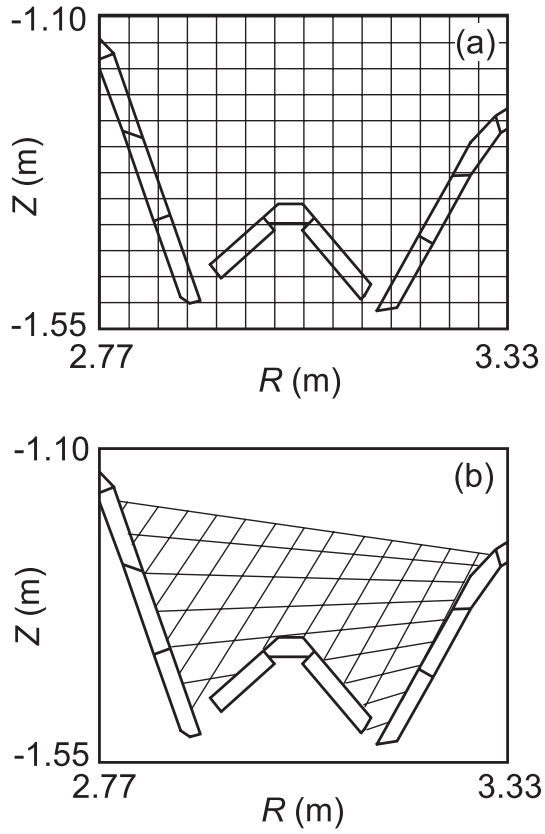

Fig. 3 The arrangement of (a) the square and (b) the oblique grid. The one-fourth of calculation cells is depicted for simplicity.

17 horizontal viewing chords. Thus, the region between the inner divertor plates and the dome is observed only by the vertical viewing chords. In the present work, a Maximum Entropy Method (MEM) [10] was employed because MEM is more tolerant of defects of viewing chords than other tomography techniques based on the Fourier transformation [11]. In addition, MEM is more tolerant of measurement error than an Algebraic Reconstruction Technique (ART) [12]. Furthermore, an oblique grid was employed in the tomographic reconstruction. On the square grid shown in Fig. 3 (a), a false geometric pattern was seen in the reconstructed image. This false pattern was suppressed in the reconstruction on an oblique grid with lines parallel to the viewing chords, shown in Fig. 3 (b) [13]. Therefore, in the present work, MEM on an oblique grid with 53×32 cells was used for the reconstruction.

3.2 Collisional-radiative model

The temporal development of $n_{\mathrm{D}(p)}$, the population density of the deuterium excited level p, is expressed by the differential equation [14],

$$\frac{\mathrm{d}}{\mathrm{d}t}n_{\mathrm{D}(p)} = -\Big\{\sum_{q<p}A(p,q) + \sum_{q\neq p}C(p,q)n_{\mathrm{e}} + S(p)n_{\mathrm{e}}\Big\}n_{\mathrm{D}(p)} + \sum_{q>p}A(q,p)n_{\mathrm{D}(q)} + \sum_{q\neq p}C(q,p)n_{\mathrm{e}}n_{\mathrm{D}(q)} + \Big\{\alpha(p)n_{\mathrm{e}} + \beta(p) + \gamma(p)\Big\}n_{\mathrm{D}^+}n_{\mathrm{e}}, \quad (1)$$

which is coupled with similar equations for other levels. Here p and q stand for levels which are determined by a principal quantum number n, and n_{e} and n_{D^+} denote electron density and deuteron density, respectively.

The spontaneous transition probability from level p to level q is denoted by $A(p,q)$. The rate coefficients for electron impact excitation if $p < q$ (de-excitation if $p > q$) and ionization are denoted by $C(p,q)$ and $S(p)$, respectively. The rate coefficients for three-body, radiative and di-electronic recombination are denoted by $\alpha(p)$, $\beta(p)$, and $\gamma(p)$, respectively. These rate coefficients are functions of electron temperature T_{e}.

On the assumption that the quasi-steady-state solution is valid, the time derivative of Eq. (1) can be set at 0 [15]. Then, the set of coupled differential equations reduces to a set of coupled linear equations. The steady-state solution for the population density of D at level p is obtained as

$$n_{\mathrm{D}(p)} = R_0(p)n_{\mathrm{e}}n_{\mathrm{D}^+} + R_1(p)n_{\mathrm{e}}n_{\mathrm{D}}, \quad (2)$$

where n_{D} denotes the ground-state density of deuterium. The first term of the right hand side of Eq. (2) is the recombining plasma component, and the second term the ionizing plasma component. Here, $R_0(p)$ and $R_1(p)$ are referred as to the recombining and the ionizing population coefficients, respectively, and are shown in Fig. 4. The recombining population coefficients increase with increase in the principal quantum number. Thus, the recombining plasma components of D_α, D_β, D_γ, and D_δ increase in that order. Similarly, the ionizing population coefficients decrease with increase in the principal quantum number. Thus, the ionizing plasma components of D_α, D_β, D_γ, and D_δ decrease in that order.

The Balmer-series line intensity ratio for the recombining plasma component is expressed with the population coefficients as follows:

$$\frac{I_0(p_1,2)}{I_0(P_2,2)} = \frac{A(p_1,2)R_0(p_1)n_{\mathrm{e}}n_{\mathrm{D}^+}}{A(p_2,2)R_0(p_2)n_{\mathrm{e}}n_{\mathrm{D}^+}} = \frac{A(p_1,2)R_0(p_1)}{A(p_2,2)R_0(p_2)}. \quad (3)$$

Here, $I_0(p,2)$ is the Balmer-series line intensity of the recombining plasma component in a transition from p to 2. Similarly, the Balmer-series line intensity ratio for the ionizing plasma component is expressed as follows,

$$\frac{I_1(p_1,2)}{I_1(P_2,2)} = \frac{A(p_1,2)R_1(p_1)n_{\mathrm{e}}n_{\mathrm{D}}}{A(p_2,2)R_1(p_2)n_{\mathrm{e}}n_{\mathrm{D}}} = \frac{A(p_1,2)R_1(p_1)}{A(p_2,2)R_1(p_2)}. \quad (4)$$

Here, $I_1(p,2)$ is the Balmer-series line intensity of the ionizing plasma component in a transition from p to 2. The calculated intensity ratios of $\mathrm{D}_\beta(n = 2 \leftarrow 4)$ to $\mathrm{D}_\alpha(n = 2 \leftarrow 3)$ are shown in Fig. 5 (a). In the electron temperature range below 200 eV and in the electron density range between $5 \times 10^{18}\,\mathrm{m}^{-3}$ and $5 \times 10^{20}\,\mathrm{m}^{-3}$, the intensity ratio of D_β to D_α of the ionizing plasma component

is lower than 0.14. The same intensity ratio of the recombining plasma component depends on the electron temperature and density, in particular in the electron temperature range below 10 eV. In Fig. 5 (b), the calculated intensity ratio of $D_\delta(n = 2 \leftarrow 6)$ to $D_\gamma(n = 2 \leftarrow 5)$ are shown. The intensity ratio of the ionizing plasma component is lower than 0.23. If the electron density range is higher than 5×10^{19} m^{-3}, the intensity ratio of the recombining component does not depend significantly on the electron density significantly, indicating that this is a good measure of the electron temperature.

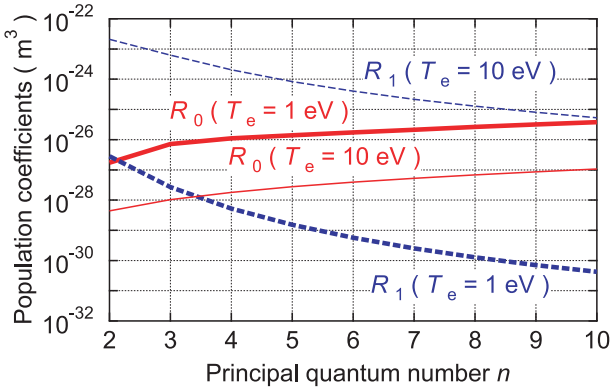

Fig. 4 Population coefficients at $n_e = 1.0 \times 10^{20}$ m^{-3} as a function of the principle quantum number, n. Solid and broken lines indicate the recombining population coefficient R_0 and the ionizing population coefficient R_1, respectively. Thick and thin lines indicate the population coefficients at $T_e = 1.0$ eV and 10 eV, respectively.

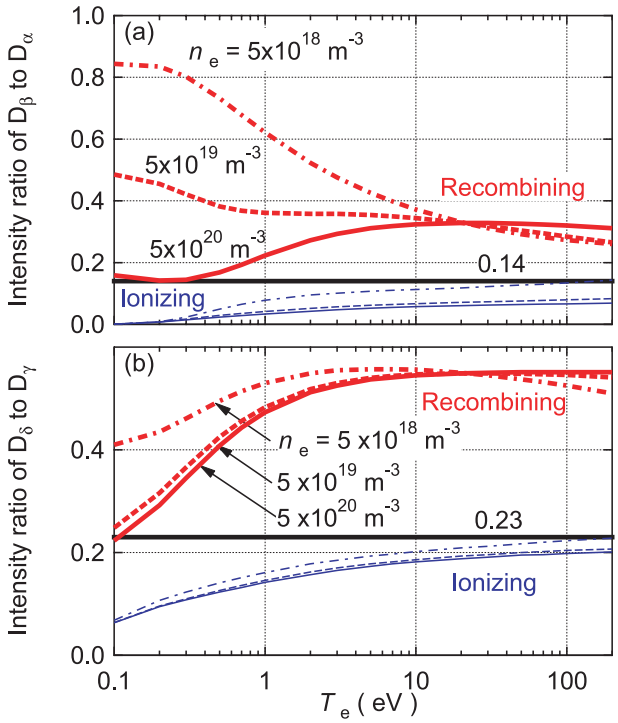

Fig. 5 The intensity ratios of (a) D_β to D_α and (b) D_δ to D_γ, calculated by a collisional-radiative model as a function of electron temperature. Thick and thin lines indicate the intensity ratios for the recombining and the ionizing plasma component, respectively.

4. Results and Discussion

Figure 6 shows the spectrum measured at 6.0 s along 88 ch of the horizontal array, where the highest D_α line emission intensity was observed. The deuterium Balmer-series line emissions from $D_\alpha(n = 2 \leftarrow 3)$ to $D_\delta(n = 2 \leftarrow 6)$ were observed with sufficiently high signal-to-noise ratio (S/N) to reconstruct the two-dimensional distributions. However, the intensities of the transitions with the upper level $n > 6$ such as $D_\varepsilon(n = 2 \leftarrow 7)$ were too weak for the tomographic reconstruction because the wavelengths of these lines were distributed in the ultra violet range, where the transmittance of the optical fiber was very low. Hence, in the present work, the tomographic reconstruction was performed for D_α, D_β, D_γ and D_δ.

The line-integral spatial profile of the D_α line emission at 6.0 s is shown in Fig. 7. The peak at 10 ch of the vertical array and the peak at 87 ch of the horizontal array suggest that a peak of the D_α line emission was located above the inner strike point. Figure 8 shows the two-dimensional distribution reconstructed from the line-integral D_α line emission shown in Fig. 7. As expected from the line-integral profile, a peak of the D_α line emission was found on the divertor plate inward from the inner strike point. A similar reconstructed two-dimensional distribution was obtained for the D_β line emission.

From these two reconstructed two-dimensional distributions, the two-dimensional intensity ratio distribution of D_β to D_α was calculated. As shown in Fig. 9 (a), the intensity ratio of D_β to D_α was higher than 0.14 around the D_α emission peak. Figure 5 (a) shows that the intensity ratio higher than 0.14 cannot be due to the ionizing plasma com-

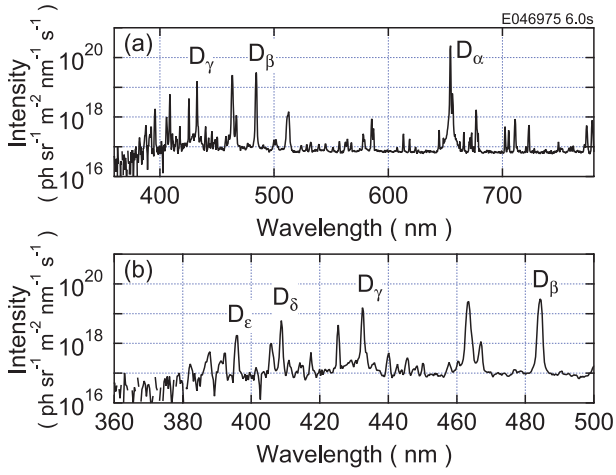

Fig. 6 (a) The spectrum measured along 88 ch, and (b) the expanded spectrum between 360-500 nm.

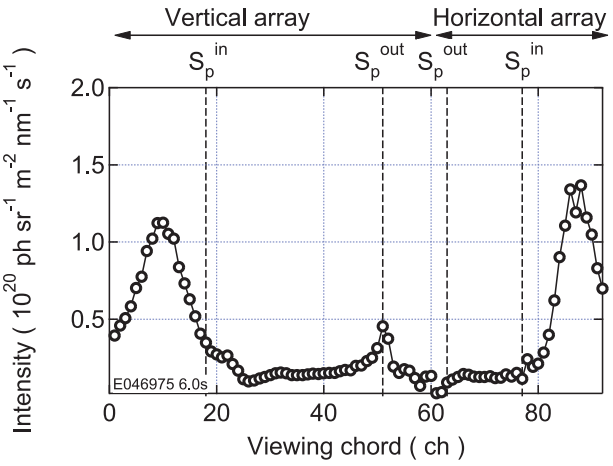

Fig. 7 The line-integral spatial distribution of the D_α line emission. The inner and the outer strike point are indicated by S_p^{in} and S_p^{out}, respectively.

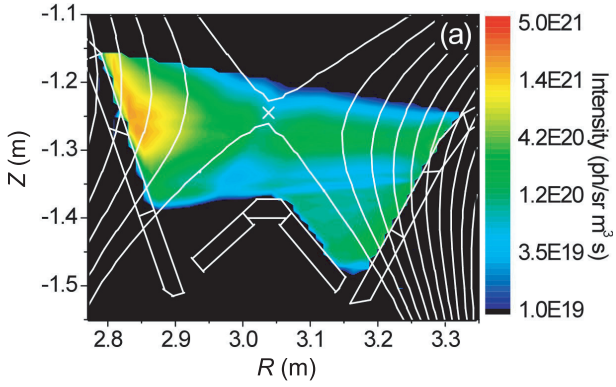

Fig. 8 Reconstructed two-dimensional distribution of the D_α line emission at 6.0 s.

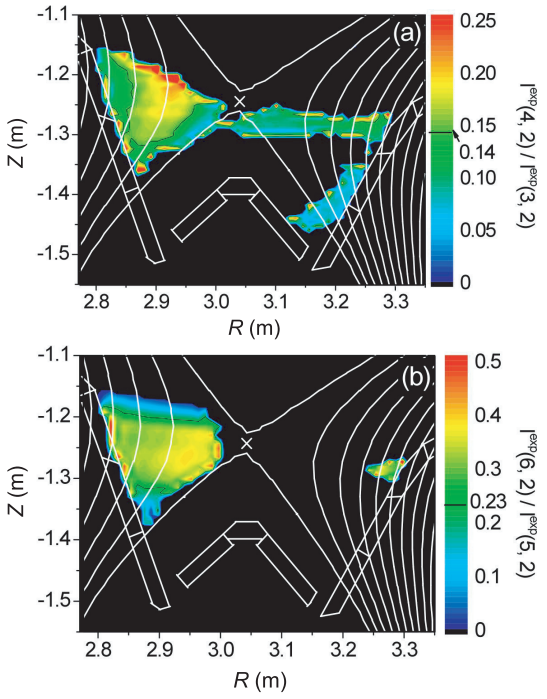

Fig. 9 The two-dimensional intensity ratio distribution of (a) D_β to D_α and (b) D_δ to D_γ calculated from the reconstructed two-dimensional distributions. The solid line represents an intensity ratio of (a) 0.14 and (b) 0.23.

ponent alone, indicating that a recombining plasma component was contained in the D_β line emission.

Figure 9 (b) shows the two-dimensional intensity ratio distribution of the D_δ to the D_γ line emission. The intensity ratio was higher than 0.23 throughout the inner divertor plasma, even at the peak of the D_α line emission, unlike the intensity ratio of the D_β to the D_α line emission. This indicates that a recombining plasma component existed in the D_δ line emission throughout the inner divertor plasma. Hence, volume recombination occurred throughout the inner divertor plasma. Note that around the divertor plates and the separatrix of the inner divertor region, the intensity ratio is presumably affected by a reconstruction noise.

As already seen in Fig. 4, in the case where the ionizing and the recombining plasma coexist, the ratio of the recombining to the ionizing plasma component of D_α, D_β, D_γ, and D_δ increases in that order. Hence, the intensity ratio of the D_δ to the D_γ line emission is closer to the intensity ratio of the recombining plasma component than the intensity ratio of other line emission such as the intensity ratio of the D_β to the D_α line emission. Further, in the case where the electron density is higher than 5×10^{19} m^{-3}, the intensity ratio of the D_δ to the D_γ line emission does not depend significantly on the electron density significantly, as shown in Fig. 5 (b). This is because the population of the upper levels of these transitions (n = 5 and 6) are close to the Saha Boltzmann distribution, due to Local Thermodynamic Equilibrium (LTE). Therefore, the intensity ratio of the D_δ to the D_γ line emission is a good measure of the electron temperature in the case where the ionizing plasma component can be ignored and the electron density is higher than 5×10^{19} m^{-3}. Given that the intensity ratio of D_δ to D_γ was 0.3 ~ 0.4 throughout the inner divertor as shown in Fig. 9 (b), the electron temperature was estimated to be 0.2 ~ 0.5 eV.

Next, the assumptions introduced to estimate the electron temperature were examined by analyzing the local population at a cell of the reconstruction grid. Figure 10 shows the local populations at the cell where the emission peak was found. Because this cell is on the center of the peak, high accuracy in the tomographic reconstruction is expected. In addition, because the line-integral intensity is the highest on the viewing chords of 10 ch and 88 ch, which pass through the emission peak, the line-integral intensity should be close to the local intensity ratio obtained by the tomography, meaning that a similar population ratio should be obtained. As shown in Fig. 10, the local populations are in good agreement with the mea-

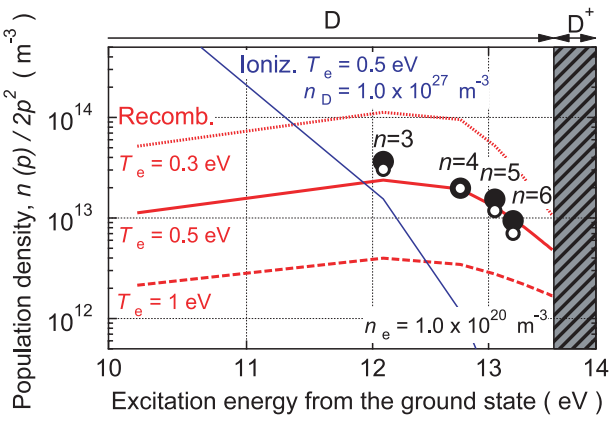

Fig. 10 The local population density at the intersection of 10 ch of the vertical array and 88 ch of the horizontal array (solid circles) and the population density of 88 ch (a line-integral length of 0.07 m is assumed) (open circles), as a function of the excitation energy from the ground state. The dotted, the solid and the broken line indicate the population density of the recombining plasma component calculated by a collisional-radiative model at $n_e = n_{D^+} = 1.0\times10^{20}$ m^{-3} and, respectively, T_e = 0.3, 0.5 and 1.0 eV. The thin solid line indicates the population density of the ionizing plasma component at $n_e = 1.0 \times 10^{20}$ m^{-3}, $n_D = 1 \times 10^{27}$ and T_e = 0.5 eV.

sured line-integral populations on the assumption that the line-integral length is 0.07 m. This line-integral length is close to the two-dimensional width of the emission peak ($\sim$ 0.1 m). These results indicate that the reconstruction of the two-dimensional distribution was successful.

Because the population ratio of these high n levels is sensitive to the electron temperature and not sensitive to the electron density under LTE, the electron temperature can be determined accurately from the population ratio. In addition, the absolute population density (not ratio) is sensitive to the electron temperature due to the electron temperature dependence of the recombination rate. For instance, the population density of $n = 4$ at $T_e = 0.5$ eV is higher and lower by a factor of 5 than, respectively, that at $T_e = 1.0$ eV and that at $T_e = 0.3$ eV. Therefore, once the electron temperature is determined from the population ratio of the $n = 4, 5$ and 6 levels, the electron density can be determined from the absolute population density. In the present work, the local population of $n = 4, 5$ and 6 is well reproduced by the populations of the recombining plasma component calculated by the collisional-radiative model with an electron temperature of 0.5 eV and density of 1.0×10^{20} m^{-3}.

However, the local population of $n = 3$ is higher by a factor of 1.5 than the calculated one, showing that another population component is contained. To compensate for this difference with the population of an ionizing plasma component with an electron temperature of 0.5 eV, an impossibly high neutral deuterium density of 1×10^{27} m^{-3} is required. This indicates that the ionizing plasma component is negligibly low in the divertor plasma parameter range, and that other different processes such as molecular assisted recombination (MAR) are involved. In Alcator C-mod, a similar result was obtained [3]; the high population of the n=3 level could not be explained by the absorption of the Lyman-series line emission, and therefore, it was concluded that the MAR process contributed to the n=3 population. It was shown that the MAR process contributed substantially to the electron-ion recombination in JT-60U [7]. The difference between the measured and calculated population density could be explained by postulating that the MAR process selectively populates the n=3 level. For this purpose, a more accurate collisional-radiative model, which can consider the collisional transitions between the excited levels of the molecule, is required.

5. Summary and Conclusions

In order to investigate the volume recombination in detached divertor plasmas, all the Balmer-series lines were measured simultaneously and two-dimensionally with a spatial resolution of $\sim$1 cm. From the line-integral intensity, the two-dimensional distributions of D_α, D_β, D_γ and D_δ were reconstructed with an improved tomographic technique on an oblique grid following the viewing chords. It was observed that the deuterium Balmer-series line emissions peaked above the inner strike point in the inner detached plasma. The two-dimensional emission ratio of D_δ to D_γ indicated that the volume recombination occurred throughout the inner divertor plasma. In particular, through comparison of the local population density at the emission peak and the population calculated by the collisional-radiative model, it was shown that the population density of high n levels (n = 4, 5 and 6) was determined by the electron-ion volume recombination with an electron temperature and density of 0.2-0.5 eV and 1×10^{20} m^{-3}, respectively, and that the population density of the n=3 level was not explained by the recombining plasma component with or without the ionizing plasma component. Presumably, the population of the n=3 level was enhanced by molecular assisted recombination processes. To investigate the population process at the n=3 level, a more detailed collisional-radiative model is required.

[1] G. Federici *et al.*, Nucl. Fusion **41**, 1967 (2001).
[2] B. Lipschultz *et al.*, Phys. Plasmas **6**, 1907 (1999).
[3] J.L. Terry *et al.*, Phys. Plasmas **5**, 1759 (1998).
[4] U. Wenzel *et al.*, Nucl. Fusion **39**, 873 (1999).
[5] D. Lumma *et al.*, Phys. Plasmas **4**, 2555 (1997).
[6] H. Kubo *et al.*, JAERI Research **039**, 139 (1998) (Japan Atomic Energy Agency).
[7] H. Kubo *et al.*, J. Nucl. Mater. **161**, 337 (2005).
[8] K. Fujimoto *et al.*, Plasma Fusion Res. **2**, S1121 (2007).
[9] T. Nakano *et al.*, Nucl. Fusion **47**, 1458 (2007).

[10] J. Skilling and R.K. Bryan, Mon. Not. Astr. Soc. **211**, 111 (1984).
[11] P. Franz *et al.*, Nucl. Fusion **41**, 695 (2001).
[12] S. Takamura *et al.*, Plasma Phys. Control. Fusion **28**, 1717 (1986).
[13] K. Fujimoto *et al.*, Trans. Fusion Sci. Tec. **51**, 247 (2007).
[14] T. Fujimoto *et al.*, *International series of monographs on physics* **123** (Oxford science publications, New York, 2004).
[15] K. Sawada and T. Fujimoto, Phys. Rev. E **49**, 5565 (1994).